

Quasi-biennial oscillation disrupted by abnormal Southern Hemisphere stratosphere

James A. Anstey^{1,1,1}, Timothy P. Banyard^{2,2,2}, Neal Butchart^{3,3,3}, Lawrence Coy^{4,4,4}, Paul A. Newman^{4,4,4}, Scott Osprey^{5,5,5}, and Corwin Wright^{2,2,2}

¹Canadian Centre for Climate Modelling and Analysis

²University of Bath

³Met Office Hadley Centre

⁴NASA Goddard Space Flight Center Greenbelt

⁵National Centre for Atmospheric Science

November 30, 2022

Abstract

The quasi-biennial oscillation (QBO) of tropical stratospheric winds was disrupted during the 2019/20 Northern Hemisphere winter. We show that this latest disruption to the regular QBO cycling was similar in many respects to that seen in 2016, but initiated by horizontal momentum transport from the Southern Hemisphere. The predictable signal associated with the QBO's quasi-regular phase progression is lost during disruptions and the oscillation reemerges after a few months significantly shifted in phase from what would be expected if it had progressed uninterrupted. We infer from an increased wave-momentum flux into equatorial latitudes seen in climate model projections that disruptions to the QBO are likely to become more common in future. Consequently it is possible that in future the QBO could be a less reliable source of predictability on lead times extending out to several years than it currently is.

Prospect of increased disruption to the QBO in a changing climate

James A. Anstey^{1*}, Timothy P. Banyard², Neal Butchart³, Lawrence Coy^{4,5},
Paul A. Newman⁴, Scott Osprey^{6,7}, Corwin J. Wright²

¹Canadian Centre for Climate Modelling and Analysis, Environment and Climate Change Canada,
Victoria, Canada

²Centre for Space, Atmospheric and Oceanic Science, University of Bath, Bath, UK

³Met Office Hadley Centre, Reading, United Kingdom

⁴NASA Goddard Space Flight Center Greenbelt, Maryland, USA

⁵SSAI, Lanham, Maryland, USA

⁶National Centre for Atmospheric Science, Oxford, United Kingdom

⁷Department of Physics, University of Oxford, Oxford, United Kingdom

Key Points:

- A second recent disruption of the quasi-biennial oscillation (QBO) has occurred.
- Large momentum fluxes from the Southern Hemisphere made a substantial contribution to the 2019/20 disruption.
- Increased equatorward momentum flux in climate model projections suggests QBO disruptions may become more likely in future.

Abstract

The quasi-biennial oscillation (QBO) of tropical stratospheric winds was disrupted during the 2019/20 Northern Hemisphere winter. We show that this latest disruption to the regular QBO cycling was similar in many respects to that seen in 2016, but initiated by horizontal momentum transport from the Southern Hemisphere. The predictable signal associated with the QBO's quasi-regular phase progression is lost during disruptions and the oscillation reemerges after a few months significantly shifted in phase from what would be expected if it had progressed uninterrupted. We infer from an increased wave-momentum flux into equatorial latitudes seen in climate model projections that disruptions to the QBO are likely to become more common in future. Consequently it is possible that in future the QBO could be a less reliable source of predictability on lead times extending out to several years than it currently is.

Plain Language Summary

The quasi-biennial oscillation (QBO) consists of a regular switching between eastward and westward winds in the tropical stratosphere. The oscillation has persisted at least since its discovery in the 1960s, over which time its period averages about 28 months with some variability from cycle to cycle. Recently, during the Northern Hemisphere winters of 2015/16 and 2019/20, remarkable departures from this regular behaviour occurred that have no precedent in the observational record. Both the 2015/16 and 2019/20 QBO disruptions occurred when large horizontal fluxes of momentum intruded into the tropics from higher latitudes. Using climate model projections we find these horizontal fluxes are likely to increase in future, suggesting an increased future likelihood of QBO disruptions and a concomitant loss in QBO predictability.

1 Introduction

The quasi-biennial oscillation (QBO) consists of alternating layers of eastward and westward wind that gradually descend through the tropical stratosphere before dissipating near the tropopause (Baldwin et al., 2001; Tegtmeier et al., 2020). The oscillation period is somewhat variable, averaging about 28 months with a standard deviation of 3–4 months (Baldwin et al., 2001; Bushell et al., 2020). The QBO dominates stratospheric variability in the tropics while modulating variability in mid to high latitudes (Anstey

& Shepherd, 2014) and thereby provides a useful source of predictability on timescales ranging from several months (seasonal) to several years ahead (Scaife, Athanassiadou, et al., 2014). The established QBO fluid dynamical mechanism involves vertically propagating waves from the troposphere that accelerate the winds when they dissipate in the tropical stratosphere (Baldwin et al., 2001), leading to descending layers of winds of opposite sign (Fig. 1a). Opposing the downward progression is tropical upwelling (Dunkerton, 1997) from the Brewer-Dobson circulation (Butchart, 2014). It has been argued that horizontally propagating waves from the mid-latitudes into the tropics play a minor part in the QBO's evolution (O'Sullivan, 1997), which is consistent with the QBO's remarkable cycle-to-cycle consistency and predictability extending out to a few years (Scaife, Athanassiadou, et al., 2014). This highly predictable QBO signal is encapsulated by the time evolution of the amplitudes of the leading two Empirical Orthogonal Functions (EOFs) of zonal wind vertical structure, which capture $\sim 90\%$ of the month-to-month variability (Wallace et al., 1993).

In February 2016 the usual QBO cycling was disrupted (Newman et al., 2016; Osprey et al., 2016; Dunkerton, 2016; Coy et al., 2017) for the first time since its discovery in the early 1960s (Ebdon & Veryard, 1961; Reed et al., 1961). A shallow layer of westward winds appeared at 40 hPa within a decaying eastward QBO phase (Fig. 1a). Anomalous westward acceleration resulted from unusually large horizontal fluxes of wave-momentum from the Northern Hemisphere (NH) (Osprey et al., 2016; Coy et al., 2017), likely related to the occurrence of a very large El Niño event (Dunkerton, 2016; Barton & McCormack, 2017). Conditions in the subtropics contributed to focusing the wave activity into the QBO jet (Hitchcock et al., 2018; Watanabe et al., 2018). Failures by models to predict the disruption (Osprey et al., 2016) are consistent with it originating in the extratropics since predictability timescales are shorter there than in the tropics. The abnormal westward winds at 40 hPa subsequently strengthened, descended, and the QBO returned to its usual cycling by early 2017, roughly a year after the disruption began (Fig. 1a).

A second QBO disruption began in December 2019, only four years after the previous event and without a strong El Niño being present. This paper makes an initial examination of the origin and evolution of this recent event by comparing the two disruptions using physical and statistical metrics. We then use future projections from climate models to assess whether QBO disruptions could potentially be an emerging signal of climate change.

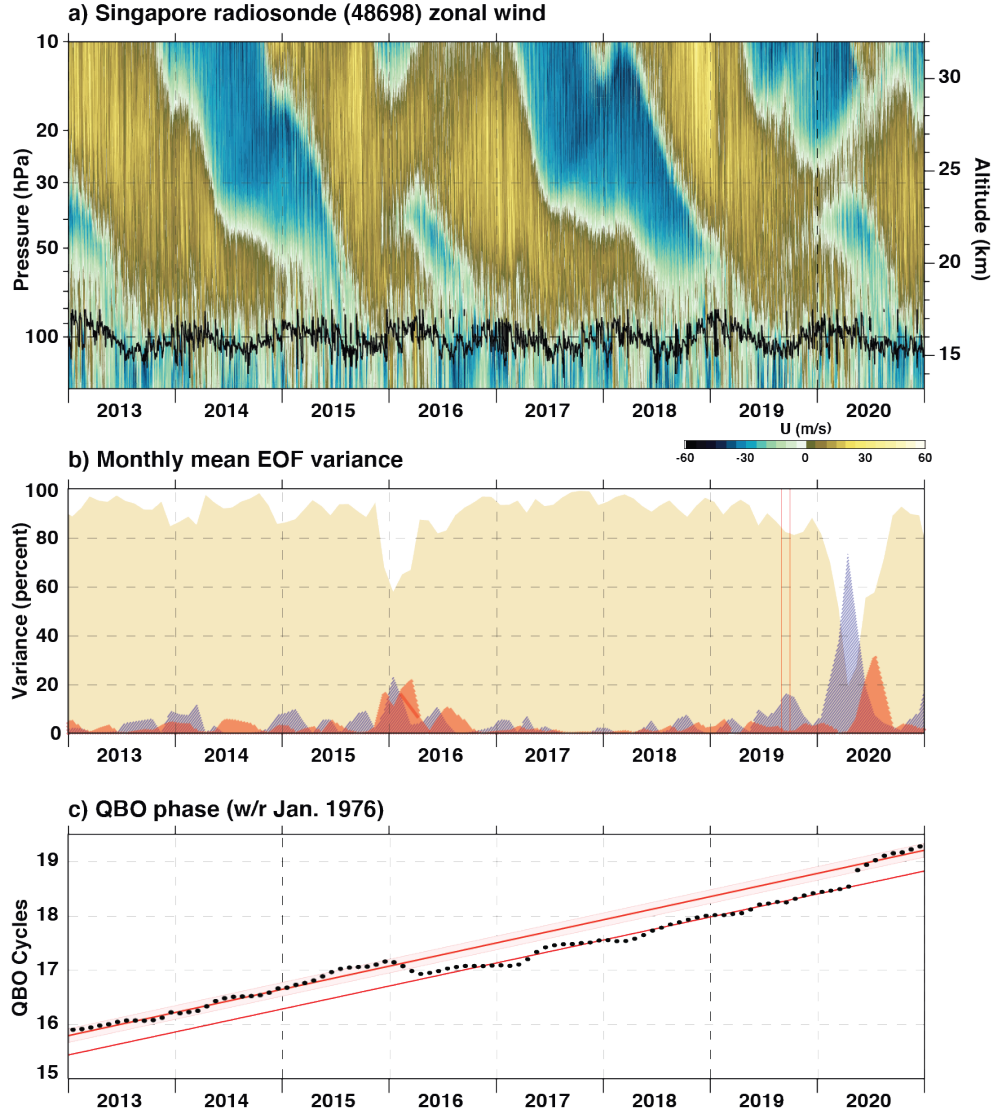


Figure 1. (a) Twice daily radiosonde zonal wind observed at Singapore (1.4° N, 104° E, station id 48698). Lapse-rate tropopause determined from the radiosonde temperatures is shown as a black line. Missing radiosonde data are filled in with MERRA-2 interpolated to the location of Singapore. (b) The percent variance explained by principal components (PCs) 1 and 2 combined (light orange shading) and PCs 3 (dark orange) and 4 (blue) as a function of time based on the monthly averaged Singapore zonal wind profiles (1976–2020) from 100–10 hPa. The EOF calculation was based on monthly averaged winds limited to 1976–2014 to avoid the two disruptions. The red vertical lines bracket September 2019. (c) Singapore QBO phase as a function of time in units scaled so that each 2π is one QBO cycle. The upper red line is fitted to the the phase from January 1976 through December 2014. The lower red line is fitted from August 2016 through December 2019. The shading about the upper red line denotes plus or minus one standard deviation. (For the complete time series going back to January 1976, see Fig. S1.)

2 Methods

Our characterization of the QBO disruption is based on a tropical rawinsonde station (Singapore, 1°N, 104°E) and global gridded analysis fields from the ERA5 reanalysis (Hersbach et al., 2020).

Daily and monthly averages of the zonal wind component are constructed from the twice daily meteorological Singapore soundings (Durre et al., 2016). The vertical structure (100–10 hPa) of the QBO is decomposed into a set of Empirical Orthogonal Functions [EOFs (Wallace et al., 1993; Dunkerton, 2016)] based on the monthly-mean zonal wind from Jan 1976–Dec 2014. The monthly winds from Jan 2013–Sep 2020 are then projected onto the first four leading EOFs as the Principal Components (PCs) and the relative variance explained by each of the PCs calculated for each month.

The ERA5 reanalysis combines a global atmospheric model with surface, aircraft, and satellite observations from 1979–present (Hersbach et al., 2020). ERA5 gridded meteorological fields on model levels at 6-hourly frequency and 2° horizontal resolution are used to calculate contributions to the zonal-mean zonal momentum budget due to wave forcing, quantified by the Eliassen-Palm (EP) flux, and advection (Andrews et al., 1987). The 6-hourly results are averaged to daily means for plotting. ERA5 model levels have ~0.5 km vertical resolution in the lower stratosphere and are exactly pressure levels from 71 hPa upward (<https://www.ecmwf.int/en/forecasts/documentation-and-support/137-model-levels>). Model level data are used because reanalysis output on the standard available pressure levels have insufficient vertical resolution for accurate calculation of vertical wind shear and other vertical gradients involved in the momentum budget calculations.

For model projections we use simulations from the SPARC (Stratosphere-troposphere Processes And their Role in Climate) QBO initiative (QBOi) (Butchart et al., 2018; Anstey et al., 2020) and from phase six of the Coupled Model Intercomparison Project (CMIP6) (Eyring et al., 2016). From the QBOi multi-model ensemble we use present-day, doubled CO₂, and quadrupled CO₂ timeslice simulations from 11 atmospheric general circulation models that simulate QBOs (Bushell et al., 2020; Richter et al., 2020). From the CMIP6 multi-model ensemble we use the historical and SSP5-8.5 scenarios from 10 coupled (Earth system) models that provided EP-flux diagnostics for both scenarios, which were: CanESM5, CESM2, CESM2-WACCM, GFDL-CM4, GFDL-ESM4, HadGEM3-

GC31-LL, INM-CM4-8, MIROC6, MRI-ESM2-0, UKESM1-0-LL. One realization was used per model.

3 Disruptions to regular QBO cycling

The characteristic QBO descending eastward and westward wind pattern disintegrated in 2019/20, with Singapore rawinsonde observations showing unexpected westward winds appearing near 40 hPa along with an atypical ascending layer of eastward winds (Fig. 1a). The small vertical scale of this ascending eastward layer is unique in the record. A decomposition of the QBO winds into EOFs (Sec. 2) quantifies this unusual vertical structure (Fig. 1b). The first two EOFs (encompassing the largest scale downward propagating structure of the QBO) typically explain over 90% of the vertical structure variance but their values drop drastically to $\sim 20\%$ by May 2020 as the higher order, smaller scale, EOFs 3 and 4 grow in amplitude. This extreme 2019/20 decrease in the variance explained by EOFs 1 and 2 greatly exceeds the decrease to 60% associated with the 2015/16 disruption.

The overall rate of phase change of the QBO had been remarkably stable before the 2015/16 disruption (Fig. 1c). Constant QBO phase progression represented by the upper red line in Fig. 1c provides a reasonably accurate representation of the true phase from 1976 until the 2015/16 disruption with a standard deviation of the phase until then of $\sim 45^\circ$. The 2015/16 disruption resulted in a retrogressed phase shift of $\sim 135^\circ$, well outside this standard deviation. The lower red line denotes the post-disruption constant phase progression prediction, but this again failed in early 2020 when the QBO phase rapidly increased by $\sim 135^\circ$ - coincidentally, returning close to the original phase that would have been expected based on the historical phase progression (upper red line).

4 Canonical model vs. meridional wave fluxes

For both disruptions, strong wave-forcing by meridional momentum transport (meridional EP-flux; Sec. 2) initiated an eastward-to-westward transition of the zonal-mean zonal winds in the lower stratosphere, around 40 hPa (Fig. 2). The canonical model of the QBO model explains the oscillation as resulting from a feedback between the zonal-mean zonal wind and vertical momentum transport (Lindzen & Holton, 1968; Holton & Lindzen, 1972). Momentum deposition by upward-propagating waves causes wind vertical shear zones to descend even as the Brewer-Dobson circulation moves the entire tropical stratosphere

upward (Dunkerton, 1997). Beginning in June and lasting until September 2019, westward forcing by meridional momentum transport at 50 hPa was large compared to the net forcing from vertical momentum transport and vertical advection (Fig. 2a). In the context of the 1979–2020 ERA5 record this forcing was extremely large over all QBO altitudes below the descending westward shear zone (between 70 and 20 hPa; red line and grey shading in Fig. 2c). In the canonical QBO model, waves deposit momentum in the zonal-mean flow over narrow altitude ranges where they encounter strong vertical shears. However during July–September 2019 strong deposition occurred over all altitudes of the QBO eastward phase, including those well below the descending westward shear zone (Fig. 2c).

Similar features are evident for the 2015/16 disruption (Fig. 2b,d) but with different timing. Strong forcing by meridional momentum transport at 50 hPa began in November 2015 and persisted through early February 2016 when westward winds emerged near 40 hPa (Fig. 2b). This forcing was exceptional in the context of the 1979–2020 record and it occurred within a deep eastward QBO phase (Fig. 2d). A shallow layer of westward wind shear centered at 50 hPa, that appeared in November 2015 and strengthened over the next 3 months (Fig. S2b), is clearly visible in the December–February average vertical profile (Fig. 2d, black line). In the July–September 2019 average, the beginning of a similar shear anomaly is just barely discernible as an indent in the wind profile near 50 hPa (Fig. 2c, black line). A shallow region of weak westward shear appeared near 60 hPa in September, subsequently strengthening and expanding upward during October–December (Fig. S2a) to resemble the wind shear seen at these same altitudes in December–February 2015/16 (Fig. S2b). Sustained westward forcing by meridional momentum transport continued at 40–50 hPa during October–December 2019 although it was weaker than in July–September (Fig. S2c,e) and unexceptional in the record (not shown). Strong westward forcing at 40 hPa due to vertical advection also occurred over this period (Fig. S2c; Sec. 5), associated with eastward wind shear that had strengthened at this altitude during July–September (Fig. S2a). Consequently the eastward winds near 40 hPa continued to weaken over this period (Fig. S2c) until westward winds emerged in late December 2019.

The 2019/20 QBO disruption thus resembles the 2015/16 event in that meridional momentum fluxes, neglected in the canonical QBO model, became anomalously strong and weakened the QBO eastward phase in the lowermost stratosphere, leading approx-

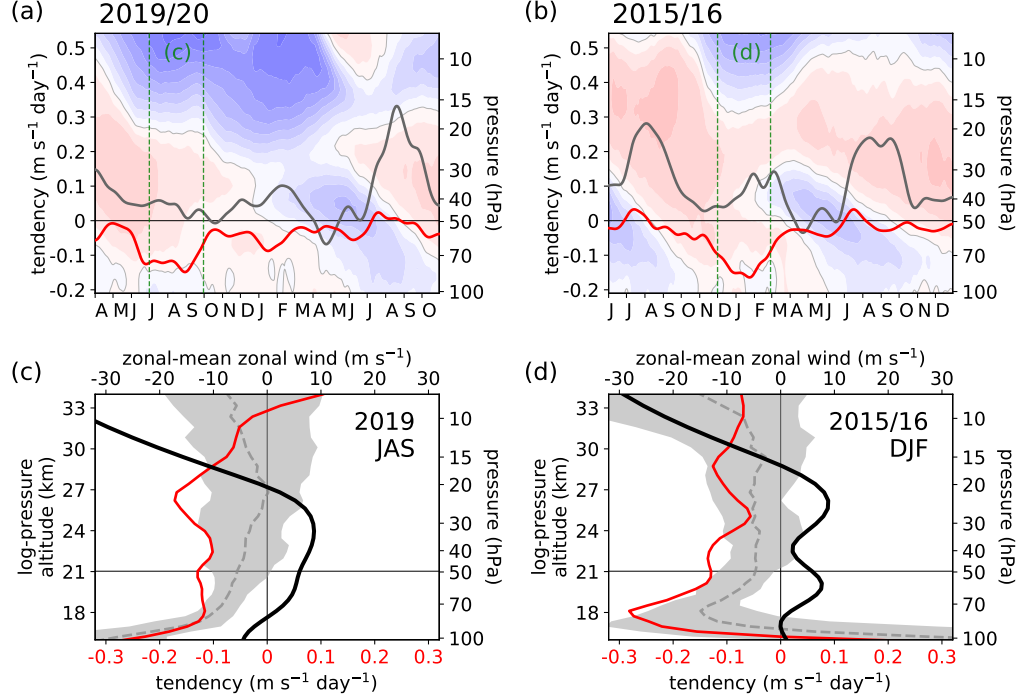


Figure 2. (a,b) Time series of ERA5 equatorial forcing tendency due to meridional EP-flux convergence (red) and the sum of vertical EP-flux convergence and vertical advection (grey) superimposed on the altitude vs. time progression of zonal-mean zonal wind (5 m s^{-1} contours, eastward red, westward blue) for (a) April 2019 to October 2020 and (b) June 2015 to December 2016. (c,d) Vertical profiles of meridional EP-flux divergence (red) and zonal-mean zonal wind (black) averaged over (c) July to September 2019 and (d) December 2015 to February 2016; the averaging periods are bracketed by vertical dashed green lines in (a,b). Grey shading shows the 5%–95% range (median dashed) of meridional EP-flux convergence over the 1979–2020 period for (c) July–September (JAS) and (d) December–February (DJF). All panels use ERA5 daily data, 4° S – 4° N average, smoothed in (a,b) with a Gaussian-weighted running mean using $\sigma=2$ days ($\sigma=10$ days) for wind (tendencies). (For the full momentum budget, see Fig. S2.)

imately three months later to the emergence of a shallow westward layer near 40 hPa. In both events this forcing occurred near the bottom of the eastward QBO phase, well below the descending westward phase above. The peak wind speed reached in the shallow westward layer was similar in both cases, being -21 m s^{-1} in 2019/20 and -19 m s^{-1} in 2015/16 (Fig. 2a,b). The two events differed in the timing of the strongest forcing by meridionally propagating waves: during Southern Hemisphere (SH) winter for the 2019/20 disruption, and during NH winter for the 2015/16 disruption. Forcing strengths also differed: peak forcing was stronger in 2015/16 (Fig. 2a and 2b, red lines) but concentrated over a shorter period from when the QBO eastward phase began its decay to when the 40 hPa westward layer emerged. At 50 hPa the time-integrated forcing from June to December 2019 was roughly 30% larger than that from October 2015 to February 2016 (-17 m s^{-1} and -13 m s^{-1} , respectively) but was spread over a longer period (Fig. S3).

5 Role of Southern Hemisphere in 2019/20 disruption

Rossby waves propagate upward and equatorward from their extratropical source regions, but the tropical stratosphere is usually shielded from their incursions by a region of westward or weak eastward zonal wind in the subtropical stratosphere. This was the case near 20 hPa in July–September 2019 when the wind near 20° S was very strongly westward compared to the other years between 1979–2020 (Fig. 3a). In contrast, near 70 hPa the SH subtropical winds were very strongly eastward compared to other years (Fig. 3b). Consequently, this allowed for an exceptionally large northward wave-momentum flux (meridional EP-flux) from 20° S to the equator at 50 hPa (Fig. 3c). Since Rossby waves cannot propagate into westward summer hemisphere winds, this caused large westward momentum flux convergence at the equator and corresponding westward tendency (Fig. 2a,c).

Similarly, during the previous disruption equatorward wave propagation was inhibited during December–February 2015/16 by a westward NH subtropical barrier at higher altitudes (Fig. 3d) but was favoured by NH subtropical winds at lower altitudes that were very strongly eastward compared to other years (Fig. 3e), allowing an anomalously large equatorward wave-momentum flux at 50 hPa (Fig. 3f). In contrast the equatorward flux from the NH in December–February 2019/20 was unremarkable, close to the median value for 1979–2020 (Fig. 3f), indicating the importance of SH forcing for the 2019/20 event. Both disruptions occurred when subtropical winds favoured equatorward Rossby wave

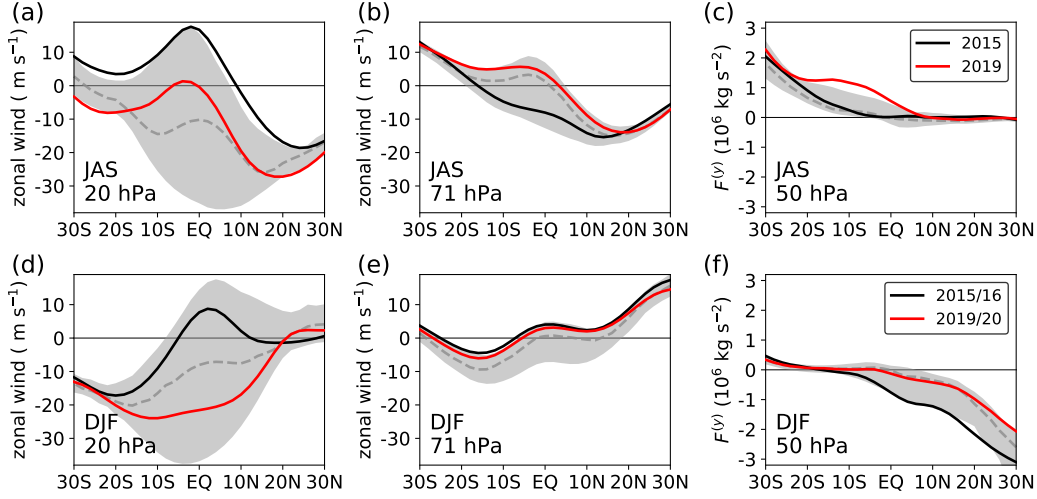


Figure 3. Meridional profiles of ERA5 (a,b) zonal-mean zonal wind and (c) meridional EP-flux, averaged over July–September (JAS) at the indicated pressure levels. (d,e,f) As (a,b,c) but averaged over December–February (DJF). The most recent (red) and previous (black) disruption years are highlighted in each panel. Grey shading shows the 5%–95% range (median dashed) over the 1979–2020 period for each variable at the indicated level and months.

propagation at the lowermost altitudes of the QBO but not at higher altitudes. This explains why meridional momentum flux convergence did not occur primarily at higher altitudes and accelerate the downward progression of the westward equatorial shear zones there (Fig. 2c,d).

The SH winter of 2019 was unusual in that a rare minor sudden stratospheric warming (SSW) occurred, beginning in late August (Rao et al., 2020; Shen et al., 2020). The timing of the warming roughly coincided with large westward forcing by meridional EP-flux in August and September (Fig. 2a). Concurrently, a large increase in tropical upwelling occurred, most likely due to the anomalous meridional overturning circulation associated with the SSW (Baldwin et al., 2020), leading to increased vertical advection at the equator near 40 hPa in September 2019 that contributed to the deceleration of the eastward QBO phase at that level (Fig. S2c). The displacement of the SH polar vortex during the minor warming may also have contributed to a subtropical corridor of eastward winds at 40–50 hPa over South America enabling synoptic-scale wave propagation toward the equator in late August / early September, in a manner similar to that documented for the 2015/16 disruption (Lin et al., 2019). However, further investigation will

be required to determine whether or not the occurrence of the minor warming was essential to the 2019/20 QBO disruption. In any case, large equatorward meridional momentum fluxes, whatever their proximate causes, were a common feature of both disruptions.

6 Climate change

While the 2015/16 disruption could reasonably be judged as a “once in 50-year event” a second disruption in a relatively short time raises the question of possible climate-change connections. In a warming climate the quasi-regular QBO cycling breaks down in some model projections but, in general, uncertainties in the representation of small scale gravity waves in models leads to a wide spread in QBO projections (Richter et al., 2020) and hence any projected changes in occurrences of disruptions cannot be considered reliable. On the other hand, in all multi-model QBO projections, there is an overall weakening of the oscillation in the lower stratosphere (Kawatani & Hamilton, 2013; Richter et al., 2020; Butchart et al., 2020), attributed to the well established speeding-up of the Brewer-Dobson circulation (tropical upwelling) in models in response to climate change (Kawatani & Hamilton, 2013; Butchart, 2014). A weaker QBO with eastward phase persisting longer in the lower stratosphere due to a faster Brewer-Dobson circulation is more likely to be vulnerable to the effects of extra-tropical wave fluxes penetrating the equatorial latitudes.

A reliable feature of the QBOi projections (see Sec. 2 for details) used by Richter et al. (2020) is the SH weakening and NH reversal of the climatological westward winds at the edges of the QBO during winter in response to a doubling and quadrupling of CO_2 amounts (Fig. 4a). This reduces the shielding of the QBO from the effects of the Rossby waves propagating from the winter hemisphere (O’Sullivan, 1997) and consequently there is an increase, on average, in the wave momentum flux into the tropics at all levels above 60 hPa (Fig. 4b). For $4 \times \text{CO}_2$ the highest percentage increase in momentum flux is 51% at 40 hPa compared to 29% (28%) at 20 (40) hPa for $2 \times \text{CO}_2$. For the SH the maximum percentage increases again occur at 40 and 20 hPa for $4 \times \text{CO}_2$ (33%) and $2 \times \text{CO}_2$ (25%), respectively.

Changes seen in state-of-the-art climate model projections used for the latest IPCC assessment (Eyring et al., 2016) between the historical period 1961–2000 and 2061–2100 under the Shared Socioeconomic Pathways (Gidden et al., 2019) (SSP) 5-8.5 (Fig. 4c and

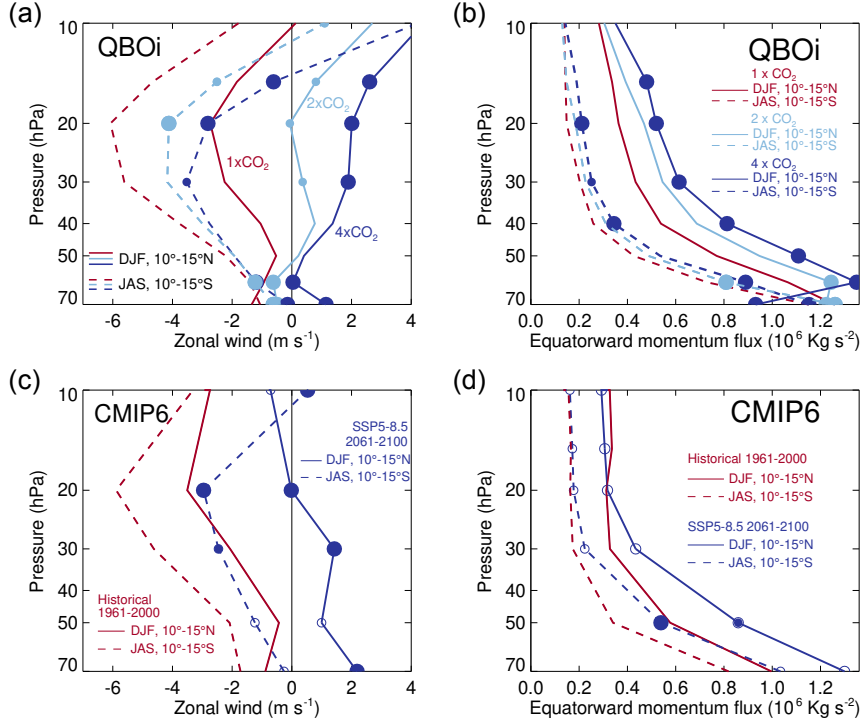


Figure 4. Projected changes in subtropical zonal-mean zonal wind and meridional EP-flux.

(a) Present-day (red), doubled CO₂ (light blue) and quadrupled CO₂ (dark blue) vertical profiles of subtropical zonal-mean zonal wind for the NH during winter (solid; averaged December–February, 10°–15° N) and the SH during winter (dashed; averaged July–September, 10°–15° S) for QBOi models. Filled circles indicate differences between present and future model ensembles that are significant at 95% (large circles) and 90% (small circles), based on a Student’s t-test.

(b) As (a) but for equatorward-directed EP-flux component (southward for the NH, northward for the SH).

(c,d) As (a,b) but historical (red) and SSP5-8.5 scenario (dark blue) simulations by CMIP6 models.

d) agree remarkably well with the QBOi projected weakening and reversal of the westward wind at the edge of the tropics (cf., Fig. 4a and c) and the projected increase of wave momentum entering the tropics (cf., Fig. 4b and d). Similar agreement was also obtained for the SSP3-7.0 scenario but because only a limited number of models uploaded momentum flux diagnostics the results are not included here. Differences between the QBOi and CMIP6 projections largely occur above 20 hPa where, for example, the CMIP6 results show no increase in the momentum flux which is possibly due to additional changes in stratospheric ozone in the CMIP6 models not included in the idealised QBOi simulations. However a detailed analysis of the differences between the two multi model ensembles is quite beyond the scope of the present study. For the SSP5-8.5 scenario the greatest percentage increase in the momentum flux was at 50 hPa (40 hPa is not included in the output levels for the CMIP6 data) with 49% and 58% increases in the NH and SH respectively, consistent with the QBOi projections. The interannual variability (standard deviation) of the monthly mean fluxes also increased, on average, in the CMIP6 projections and combined with the increase in the mean this implies a greater proportion of winters are likely to have sufficiently anomalous fluxes to disrupt the QBO. Using this novel approach of examining the more reliable response to climate change of the wave momentum fluxes rather than the simulated QBOs per se, plus the already established speeding up of the Brewer-Dobson circulation (Butchart, 2014) and weakening of QBO amplitudes (Kawatani & Hamilton, 2013; Richter et al., 2020; Butchart et al., 2020), enables us to infer with some confidence that QBO disruptions are likely to become more common due a changing climate.

7 Conclusions

The quasi-biennial oscillation has been disrupted again for only the second time since its discovery. Both disruptions occurred near 40 hPa and were initiated by historically large forcing from extratropical waves. The 2019/20 event differs in that the largest wave disturbances originated from the SH rather than the NH, no strong El Niño event was present, and an eastward jet subsequently emerged above the shallow westward layer.

The high predictability of the QBO on 3–4 year timescales can potentially provide a source of long-term (seasonal to interannual) predictive skill due to QBO teleconnections (Baldwin et al., 2001; Anstey & Shepherd, 2014; Scaife, Athanassiadou, et al., 2014; Scaife, Arribas, et al., 2014; Son et al., 2017; Gray et al., 2018; Mundhenk et al., 2018).

When this predictability disintegrates, as occurred in the 2015/16 and 2019/20 disruptions, the accuracy – and hence value to society – of such forecasts may be reduced. Following both disruptions the normal QBO cycling resumed, manifesting in 2020 as an eastward jet emerging above the shallow westward layer, consistent with the standard QBO paradigm (see Fig. S4) and auguring a return to the high predictability of the QBO until meteorological conditions once again favour disruption. By the end of 2020 the QBO had returned to a typical eastward pattern, at a similar stage in its cycle as when the chain of events leading to the disruption first began unfolding approximately a year and a half earlier (Figs. 1a & 2a).

Whether disruptions themselves can be predicted more than ~ 1 month in advance remains an open question (Watanabe et al., 2018). The 2015/16 disruption was not predicted by operational seasonal forecasting systems (Osprey et al., 2016) and early indications are that the same is true of the 2019/20 disruption, although models may perform better at predicting the evolution of the disruption once it has begun (Watanabe et al., 2018). Predicting the full “life cycle” of QBO disruptions could provide a stringent test of models. Such work will be aided by the availability of new Aeolus satellite wind observations that will monitor the evolution of the QBO over the whole tropical belt (Witschas et al., 2020). Inherently shorter predictability of disruptions (as contrasted with the usual QBO) is consistent with their extratropical origins, since the extratropics are less predictable than the tropics.

Under climate change, Rossby wave propagation into the low-latitude stratosphere is expected to increase (Shepherd & McLandress, 2011) and we have shown this occurs in model climate projections including those supporting the latest Intergovernmental Panel on Climate Change (IPCC) assessment. Under increasing influence from the extratropics, tropical stratospheric winds will likely become less predictable, leading to less skillful seasonal forecasts. Combined with an increasing Brewer-Dobson circulation (Butchart, 2014) and weakening QBO amplitudes (Kawatani & Hamilton, 2013; Richter et al., 2020; Butchart et al., 2020), the prospect of QBO disruptions is likely to increase in a changed climate.

Acknowledgments

ERA5 data were obtained from the Copernicus Data Store. The Singapore soundings were obtained from the NOAA IGRA2 data center. The climate model data used was

obtained from the CMIP6 international archive (<https://esgf-index1.ceda.ac.uk/projects/cmip6-ceda/>) and the QBOi multi-model archive at the UK Centre for Environmental Data Analysis (CEDA) (Butchart et al., 2018). NB was supported by the Met Office Hadley Centre Programme funded by BEIS and Defra and the UK-China Research & Innovation Partnership Fund through the Met Office Climate Science for Service Partnership (CSSP) China as part of the Newton Fund. LC was supported by the NASA Modeling and Analysis Program. PN was supported by the NASA Atmospheric Composition Modeling and Analysis Program. SO was supported by the National Centre for Atmospheric Science and UK NERC (NE/P006779/1, NE/N018001/1). CW was funded by the Royal Society, University Research Fellowship (UF160545). TB was funded by an EPSRC Doctoral Training Account. We thank Adam Scaife for updating us on the UK Met Office Seasonal Forecasts for the 2019/20 winter.

References

- Andrews, D. G., Holton, J. R., & Leovy, C. B. (1987). *Middle Atmosphere Dynamics*. Academic, San Diego, Calif.
- Anstey, J. A., Butchart, N., Hamilton, K., & Osprey, S. M. (2020). The sparc quasi-biennial oscillation initiative. *Quarterly Journal of the Royal Meteorological Society*, *n/a*(*n/a*). Retrieved from <https://rmets.onlinelibrary.wiley.com/doi/abs/10.1002/qj.3820> doi: 10.1002/qj.3820
- Anstey, J. A., & Shepherd, T. G. (2014). High-latitude influence of the quasi-biennial oscillation. *Quarterly Journal of the Royal Meteorological Society*, *140*(678), 1–21.
- Baldwin, M. P., Ayarzagüena, B., Birner, T., Butchart, N., Charlton-Perez, A. J., Butler, A. H., ... et al. (2020). Sudden stratospheric warmings. *Earth and Space Science Open Archive*, *49*. doi: 10.1002/essoar.10502884.1
- Baldwin, M. P., Gray, L. J., Dunkerton, T. J., Hamilton, K., Haynes, P. H., Randel, W. J., ... Takahashi, M. (2001). The quasi-biennial oscillation. *Rev. Geophys.*, *39*, 179–229.
- Barton, C. A., & McCormack, J. P. (2017). Origin of the 2016 QBO disruption and its relationship to extreme el niño events. *Geophysical Research Letters*, *44*(21), 11,150–11,157. doi: 10.1002/2017GL075576
- Bushell, A. C., Anstey, J. A., Butchart, N., Kawatani, Y., Osprey, S. M., Richter,

- 353 J. H., ... Yukimoto, S. (2020). Evaluation of the Quasi-Biennial Oscillation in
354 global climate models for the SPARC QBO-initiative. *Quart. J. Roy. Meteor.*
355 *Soc., Accepted.*
- 356 Butchart, N. (2014). The Brewer-Dobson circulation. *Reviews of Geophysics*, 52(2),
357 157–184. doi: 10.1002/2013RG000448
- 358 Butchart, N., Anstey, J. A., Hamilton, K., Osprey, S., McLandress, C., Bushell,
359 A. C., ... Yukimoto, S. (2018). Overview of experiment design and compar-
360 ison of models participating in phase 1 of the sparc quasi-biennial oscillation
361 initiative (qboi). *Geoscientific Model Development*, 11(3), 1009–1032. Re-
362 trieved from <https://www.geosci-model-dev.net/11/1009/2018/> doi:
363 10.5194/gmd-11-1009-2018
- 364 Butchart, N., Anstey, J. A., Kawatani, Y., Osprey, S. M., Richter, J. H., & Wu, T.
365 (2020). QBO changes in CMIP6 climate projections. *Geophysical Research*
366 *Letters*, 47(7), e2019GL086903. doi: 10.1029/2019GL086903
- 367 Coy, L., Newman, P. A., Pawson, S., & Lait, L. R. (2017). Dynamics of the dis-
368 rupted 2015/16 quasi-biennial oscillation. *Journal of Climate*, 30(15), 5661-
369 5674. doi: 10.1175/JCLI-D-16-0663.1
- 370 Dunkerton, T. J. (1997). The role of gravity waves in the quasi-biennial oscillation.
371 *Journal of Geophysical Research: Atmospheres*, 102(D22), 26053–26076. doi:
372 10.1029/96JD02999
- 373 Dunkerton, T. J. (2016). The quasi-biennial oscillation of 2015–2016: Hiccup or
374 death spiral? *Geophysical Research Letters*, 43(19), 10,547-10,552. doi: 10
375 .1002/2016GL070921
- 376 Durre, I., Xungang, Y., Vose, R. S., Applequist, S., & Arnfield, J. (2016). Integrated
377 global radiosonde archive (IGRA), version 2. *NOAA National Centers for En-*
378 *vironmental Information*. (Accessed May 2020) doi: 10.7289/V5X63K0Q
- 379 Ebdon, R., & Veryard, R. (1961). Fluctuations in equatorial stratospheric winds.
380 *Nature*, 189(4767), 791–793.
- 381 Eyring, V., Bony, S., Meehl, G. A., Senior, C. A., Stevens, B., Stouffer, R. J., &
382 Taylor, K. E. (2016). Overview of the coupled model intercomparison project
383 phase 6 (cmip6) experimental design and organization. *Geoscientific Model De-*
384 *velopment*, 9(5), 1937–1958. Retrieved from [https://gmd.copernicus.org/](https://gmd.copernicus.org/articles/9/1937/2016/)
385 [articles/9/1937/2016/](https://gmd.copernicus.org/articles/9/1937/2016/) doi: 10.5194/gmd-9-1937-2016

- 386 Gidden, M. J., Riahi, K., Smith, S. J., Fujimori, S., Luderer, G., Kriegler, E., ...
387 Takahashi, K. (2019). Global emissions pathways under different socioeco-
388 nomic scenarios for use in cmip6: a dataset of harmonized emissions trajecto-
389 ries through the end of the century. *Geoscientific Model Development*, 12(4),
390 1443–1475. Retrieved from [https://gmd.copernicus.org/articles/12/](https://gmd.copernicus.org/articles/12/1443/2019/)
391 1443/2019/ doi: 10.5194/gmd-12-1443-2019
- 392 Gray, L. J., Anstey, J. A., Kawatani, Y., Lu, H., Osprey, S., & Schenzinger, V.
393 (2018). Surface impacts of the quasi biennial oscillation. *Atmospheric*
394 *Chemistry and Physics*, 18(11), 8227–8247. Retrieved from [https://](https://www.atmos-chem-phys.net/18/8227/2018/)
395 www.atmos-chem-phys.net/18/8227/2018/ doi: 10.5194/acp-18-8227-2018
- 396 Hersbach, H., Bell, B., Berrisford, P., Hirahara, S., Horányi, A., Muñoz-Sabater, J.,
397 ... others (2020). The era5 global reanalysis. *Quarterly Journal of the Royal*
398 *Meteorological Society*.
- 399 Hitchcock, P., Haynes, P. H., Randel, W. J., & Birner, T. (2018). The emergence
400 of shallow easterly jets within qbo westerlies. *Journal of the Atmospheric Sci-*
401 *ences*, 75(1), 21–40.
- 402 Holton, J. R., & Lindzen, R. S. (1972). An updated theory for the quasi-biennial cy-
403 cle of the tropical stratosphere. *J. Atmos. Sci.*, 29, 1076-1080.
- 404 Kawatani, Y., & Hamilton, K. (2013, may). Weakened stratospheric quasibiennial
405 oscillation driven by increased tropical mean upwelling. *Nature*, 497, 478. doi:
406 10.1038/nature12140
- 407 Lin, P., Held, I., & Ming, Y. (2019). The early development of the 2015/16 quasi-
408 biennial oscillation disruption. *Journal of the Atmospheric Sciences*, 76(3),
409 821-836. doi: 10.1175/JAS-D-18-0292.1
- 410 Lindzen, R., & Holton, J. R. (1968). A theory of the quasi-biennial oscillation. *J.*
411 *Atmos. Sci.*, 25, 1095-1107.
- 412 Mundhenk, B. D., Barnes, E. A., Maloney, E. D., & Baggett, C. F. (2018). Skillful
413 empirical subseasonal prediction of landfalling atmospheric river activity using
414 the madden–julian oscillation and quasi-biennial oscillation. *npj Climate and*
415 *Atmospheric Science*, 1(1), 2397-3722. Retrieved from [https://doi.org/](https://doi.org/10.1038/s41612-017-0008-2)
416 [10.1038/s41612-017-0008-2](https://doi.org/10.1038/s41612-017-0008-2) doi: 10.1038/s41612-017-0008-2
- 417 Newman, P. A., Coy, L., Pawson, S., & Lait, L. R. (2016). The anomalous change
418 in the qbo in 2015–2016. *Geophysical Research Letters*, 43(16), 8791-8797. doi:

- 10.1002/2016GL070373
- Osprey, S. M., Butchart, N., Knight, J. R., Scaife, A. A., Hamilton, K., Anstey, J. A., ... Zhang, C. (2016). An unexpected disruption of the atmospheric quasi-biennial oscillation. *Science*, 353(6306), 1424–1427.
- O’Sullivan, D. (1997). Interaction of extratropical rossby waves with westerly quasi-biennial oscillation winds. *Journal of Geophysical Research: Atmospheres*, 102(D16), 19461-19469. doi: 10.1029/97JD01524
- Rao, J., Garfinkel, C. I., White, I. P., & Schwartz, C. (2020). The southern hemisphere minor sudden stratospheric warming in september 2019 and its predictions in s2s models. *Journal of Geophysical Research: Atmospheres*, 125(14), e2020JD032723. Retrieved from <https://agupubs.onlinelibrary.wiley.com/doi/abs/10.1029/2020JD032723> (e2020JD032723 2020JD032723) doi: 10.1029/2020JD032723
- Reed, R. J., Campbell, W. J., Rasmussen, L. A., & Rogers, D. G. (1961). Evidence of a downward-propagating, annual wind reversal in the equatorial stratosphere. *Journal of Geophysical Research*, 66(3), 813–818.
- Richter, J. H., Butchart, N., Kawatani, Y., Bushell, A. C., Holt, L., Serva, F., ... Yukimoto, S. (2020). Response of the quasi-biennial oscillation to a warming climate in global climate models. *Quarterly Journal of the Royal Meteorological Society*, n/a(n/a). doi: 10.1002/qj.3749
- Scaife, A. A., Arribas, A., Blockley, E., Brookshaw, A., Clark, R. T., Dunstone, N., ... Williams, A. (2014). Skillful long-range prediction of european and north american winters. *Geophysical Research Letters*, 41(7), 2514-2519. Retrieved from <https://agupubs.onlinelibrary.wiley.com/doi/abs/10.1002/2014GL059637> doi: 10.1002/2014GL059637
- Scaife, A. A., Athanassiadou, M., Andrews, M., Arribas, A., Baldwin, M., Dunstone, N., ... Williams, A. (2014). Predictability of the quasi-biennial oscillation and its northern winter teleconnection on seasonal to decadal timescales. *Geophysical Research Letters*, 41(5), 1752-1758. Retrieved from <https://agupubs.onlinelibrary.wiley.com/doi/abs/10.1002/2013GL059160> doi: <https://doi.org/10.1002/2013GL059160>
- Shen, X., Wang, L., & Osprey, S. (2020, 06). The southern hemisphere sudden stratospheric warming of september 2019. *Science Bulletin*. doi: 10.1016/j.scib

- 452 .2020.06.028
- 453 Shepherd, T. G., & McLandress, C. (2011). A robust mechanism for strengthening
 454 of the brewer–dobson circulation in response to climate change: Critical-layer
 455 control of subtropical wave breaking. *Journal of the Atmospheric Sciences*,
 456 68(4), 784–797. doi: 10.1175/2010JAS3608.1
- 457 Son, S.-W., Lim, Y., Yoo, C., Hendon, H. H., & Kim, J. (2017). Stratospheric
 458 control of the madden–julian oscillation. *Journal of Climate*, 30(6), 1909–
 459 1922. Retrieved from <https://doi.org/10.1175/JCLI-D-16-0620.1> doi:
 460 10.1175/JCLI-D-16-0620.1
- 461 Tegtmeier, S., Anstey, J., Davis, S., Dragani, R., Harada, Y., Ivanciu, I., ... others
 462 (2020). Temperature and tropopause characteristics from reanalyses data in
 463 the tropical tropopause layer. *Atmospheric Chemistry and Physics*, 20(2),
 464 753–770.
- 465 Wallace, J. M., Panetta, R. L., & Estberg, J. (1993). Representation of the equato-
 466 rial stratospheric quasi-biennial oscillation in EOF phase space. *J. Atmos. Sci.*,
 467 50, 1751–1762.
- 468 Watanabe, S., Hamilton, K., Osprey, S., Kawatani, Y., & Nishimoto, E. (2018).
 469 First successful hindcasts of the 2016 disruption of the stratospheric quasi-
 470 biennial oscillation. *Geophysical Research Letters*, 45(3), 1602–1610. doi:
 471 10.1002/2017GL076406
- 472 Witschas, B., Lemmerz, C., Geiß, A., Lux, O., Marksteiner, U., Rahm, S., ...
 473 Weiler, F. (2020). First validation of aeolus wind observations by airborne
 474 doppler wind lidar measurements. *Atmospheric Measurement Techniques*
 475 *Discussions*, 1–23.

Supporting Information

Fig. S1 shows the full 1976–2020 progression of QBO phase using Singapore radiosonde winds, of which a subset is shown in Fig. 1c. The linear slope over most of the record indicates the usual high predictability of QBO phase. The 2015/16 and 2019/20 disruptions appear as abrupt deviations from the usual phase progression.

Fig. S2 compares the evolution of ERA5 zonal-mean zonal wind and its vertical shear in the 2015/16 and 2019/20 disruption events (Fig. S2a,b) and details of the zonal-mean zonal momentum budget at 41 hPa and 50 hPa (Fig. S2c–f). More precisely the pressure levels shown are 40.53 hPa and 49.60 hPa, the closest ERA5 levels to 40 and 50 hPa. The resolved forcing terms are the meridional EP-flux component, vertical EP-flux component, meridional advection, and vertical advection. The “canonical model” forcing shown in Fig. 2a,b (grey line) is the sum of the vertical EP-flux and vertical advection at 50 hPa as shown in Fig. S2e,f. The time axis in Fig. S2 places the “central date” of each disruption at the same relative position on the axis for both disruptions. This is the time at which ERA5 zonal-mean zonal winds turned westward at 40 hPa, determined as 21 December 2019 and 1 February 2016 for the two events.

Fig. S3 shows the time integral of forcing tendency due to meridional EP-flux for the two disruptions. The total forcing by horizontal wave-momentum flux provides an alternate metric for the “strength” of the disruption, complementary to the EOF-based metric shown in Fig. 1b.

Fig. S4 indicates the resumption of typical QBO behaviour following the 2019/20 disruption. The westward wind layer at ~ 40 hPa inhibits upward-propagating tropical waves that would otherwise force the descent of the overlying westward QBO phase, which then stalls and is carried upward by the Brewer-Dobson circulation (Fig. 2a,b). When the westward winds descend to ~ 70 hPa, the barrier to upward-propagating waves with eastward phase speeds is removed. Following 2015/16 disruption this led to the resumption of eastward phase descent in April 2016. Following the 2019/20 disruption it led to an eastward jet emerging in May 2020 at ~ 25 hPa forced by the vertical EP-flux component (Fig. S4), of which $\sim 50\%$ is due to large-scale waves ($k = 1-10$; not shown), consistent with radiative damping of Kelvin waves as they encounter eastward wind shear.

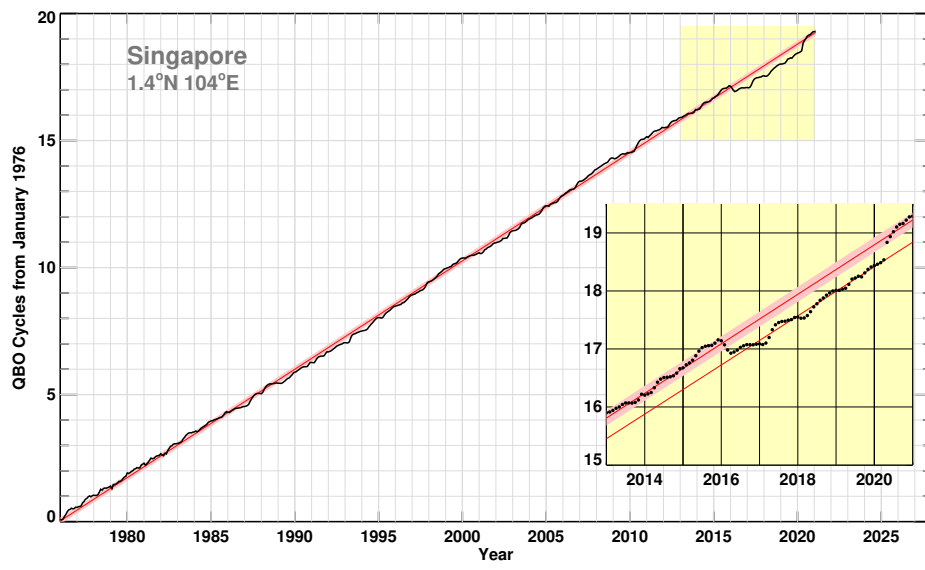


Figure S1. Singapore QBO phase as in Fig. 1c, but showing the full record since January 1976.

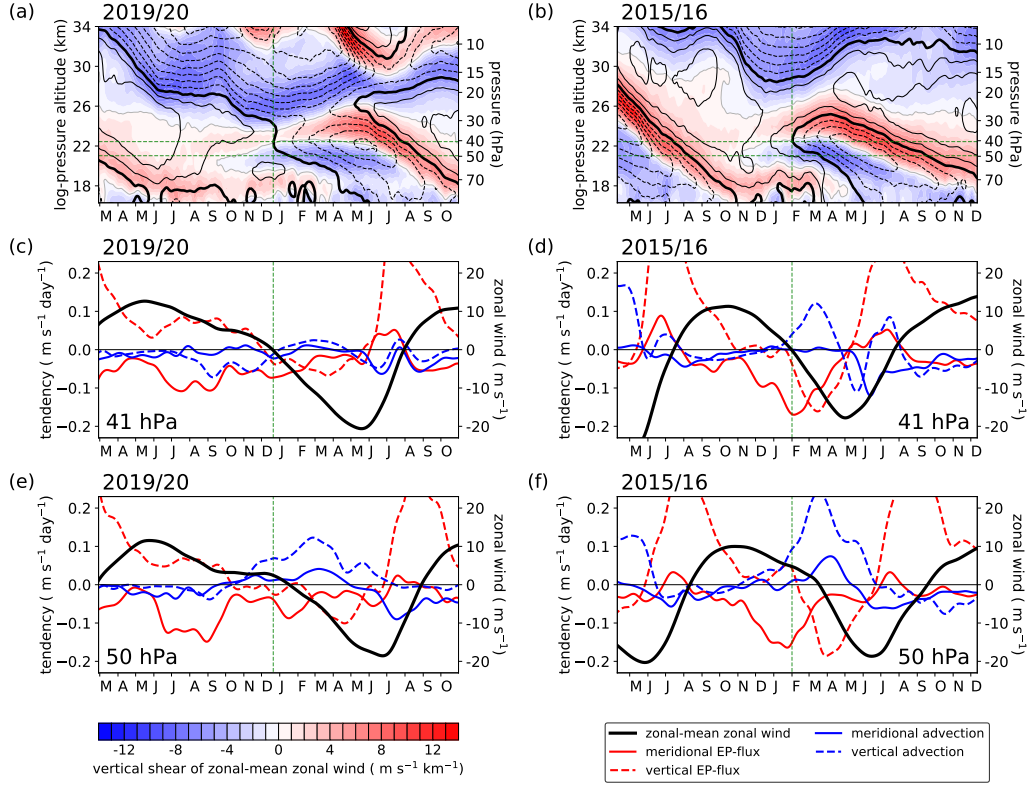


Figure S2. QBO disruptions as seen in the ERA5 reanalysis during (a,c,e) 2019/20 and (b,d,f) 2015/16. (a,b) Zonal-mean zonal wind (black contours; zero thick, westward dashed, 5 m s^{-1} spacing) and its vertical shear (filled contours). (c,d) Zonal-mean zonal wind tendency due to eddy momentum transports and advection, and zonal-mean zonal wind (thick black line) at 41 hPa. (e,f) As (c,d), but at 50 hPa. Vertical green dashed lines mark the time when westward winds first emerge near 40 hPa for each disruption. Horizontal green dashed lines in (a,b) indicate 41 and 50 hPa, the altitudes shown in (c-f). All panels use ERA5 daily means, 4° S – 4° N average, smoothed with a Gaussian-weighted running mean using (a,b) $\sigma=2$ days, (c-f) $\sigma=10$ days.

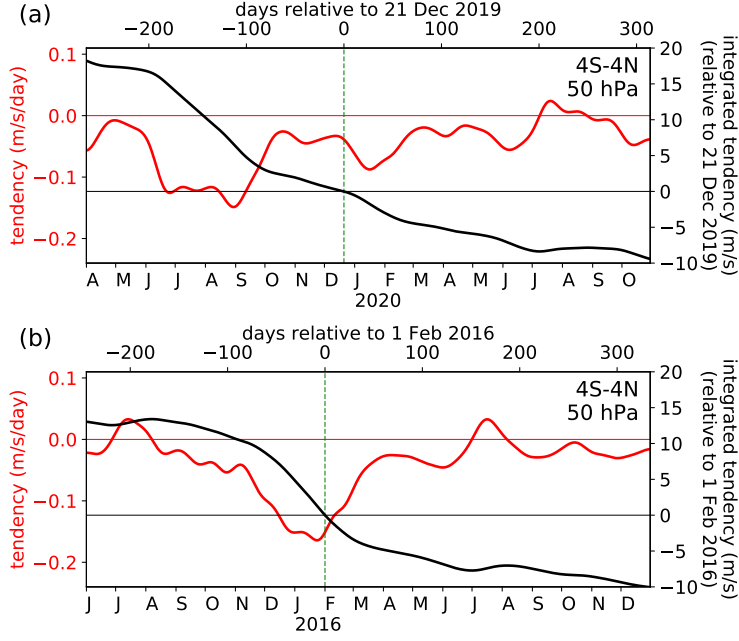


Figure S3. (a) Time-integrated zonal-mean zonal wind tendency (black) due to forcing by meridional EP-flux (red) for the 2019/20 disruption. Red curve is the same as in Fig. 2a (50 hPa, 4°S – 4°N , daily ERA5 data smoothed with $\sigma=10$ day Gaussian-weighted running mean). The black curve is the time integral of the red curve. (b) As (a) but for the 2015/16 disruption. Red curve is the same as in Fig. 2b.

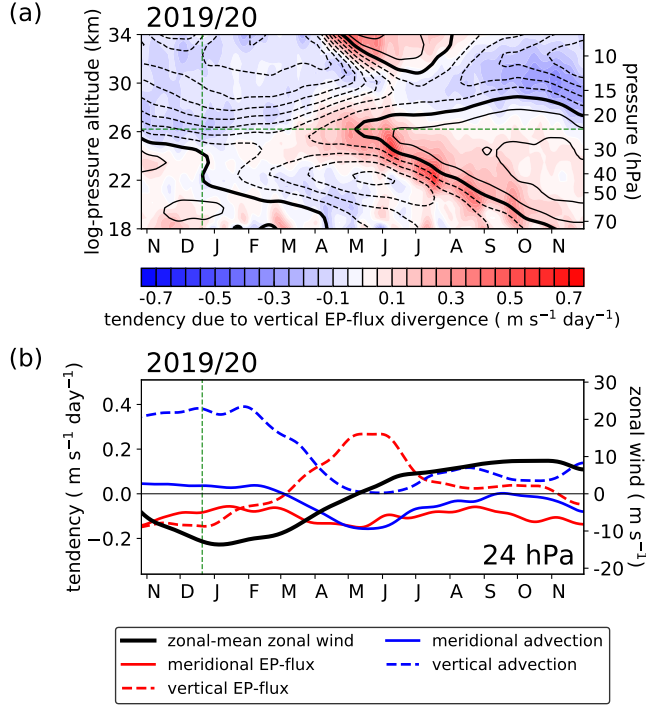


Figure S4. (a) Zonal-mean zonal wind (black contours; zero thick, westward dashed, 5 m s^{-1} spacing) and wind tendency due to vertical EP-flux component (filled contours). (b) Zonal-mean zonal wind tendency due to eddy momentum transports and advection, and zonal-mean zonal wind (thick black line), at the altitude of emerging eastward winds. Vertical green dashed line marks the time when westward winds first emerge near 40 hPa. Horizontal green dashed line in (a) indicates the altitude shown in (b). All panels use daily ERA5 daily, 4° S – 4° N average, smoothed with a Gaussian-weighted running mean using (a) $\sigma=4$ days, (b) $\sigma=10$ days.